Characterising Backscattered Electrons in EBCMOS

Xuening Wang, De Song, Gangcheng Jiao, Ye Li, and Weijun Chen

***Abstract*—The characteristics of backscattered electrons near the surface of a back-side bombarded CMOS (BSB-CMOS) within an electron bombarded CMOS (EBCMOS) were studied based on the principle of electron-solid interactions and Monte-Carlo simulation method. We mainly focused on the angular distributions of backscattered electrons, the ratio of backscattered electron number to incident electron number (RBI), and the distribution of the distance between backscattered electrons and incident electrons (D_{BI}). We studied how these characteristics were affected by the BSB-CMOS surface structure and incident electron energy. Firstly, RBI and the mean D_{BI} vary with the incident electron energy, the surface material type, and passivation layer thickness. Meanwhile, a lower RBI may reduce device noise originating from backscattered electrons (N_{BE}) due to the smaller number of backscattered electrons. Besides, the lower mean D_{BI} may enhance the device resolution, because the backscattered electron beam is more concentrated. The distribution of backscattered azimuths (Φ_{B}) and the backscattered angle (θ_{B}) follow uniform distribution and cosine angular distribution respectively, which are difficult to change. Finally, devices with the lowest RBI and a low mean value of D_{BI} were achieved when the BSB-CMOS surface was modified with 60 nm Al_2O_3 and the incident electrons were at 4 keV, which might improve the N_{BE} and resolution of the EBCMOS. This study will provide a theoretical foundation for the fabrication of high-resolution EBCMOS.**

***Index Terms*—Backscattered electron, EBCMOS, electron-solid interactions.**

I. Introduction

ELECTRON bombarded CMOS (EBCMOS) is a new type of low-light-level camera sensor technology, from which the image information can be digitally read out [1]. Compared with intensified CCDs (ICCDs), EBCMOS has attracted much attention owing to its advantages of reduced sensor size and weight, increased sensitivity and dynamic range, faster response time, and better contrast and resolution [2]. EBCMOS sensors were first developed for night vision devices in the military [1], [3]. Except for low-light-level imaging, EBCMOS cameras could also be useful in fluorescence microscopy, astronomy, high energy-physics, bioluminescence data acquisition and medical imaging [4], [5], [6], [7]. For scientific research, the development of EBCMOS cameras originated from applications in particle physics: Mimosa 5 was demonstrated in 2007, with 1024 × 1024 pixels, 40 Hz frame rate and an operating voltage of 6–10 kV [8].

The structure of the EBCMOS mainly consists of BSB-CMOS, photocathode, and vacuum tube. The photoelectrons converted by the photocathode are accelerated by the applied strong electric field between the photocathode and CMOS anode, and are directly injected into the BSB-CMOS. Recently, most of the theoretical studies on the EBCMOS have focused on the charge collection efficiency and secondary electrons gain in the multiplier layer [9], [10], [11], [12], [13]. However, when the incident electrons are accelerated (bombarded) into the surface of a solid, some of them will be scattered back into the vacuum as a result of their interaction with atoms in the solid [14], [15], [16], [17]. Here, these electrons scattered back into the vacuum, they are defined as backscattered electrons. The ratio of backscattered electron number to incident electron number (RBI) quantifies the probability that an incident electron would exit from a solid, which is a key parameter describing the backscattered electron characteristics [18], [19]. Some reports reveal that the value of RBI will change when the high energy electrons are injected into different types and thicknesses of ion barrier film in a microchannel plate image intensifier [20], [21]. To obtain the distribution of the secondary electrons, some studies have also measured the scattering properties of high energy electrons in a EBCMOS electron multiplier layer. [22], [23], [24]. A backscattered electron that is emitted into the vacuum will be injected into the BSB-CMOS as an incident electron, due to the proximity-focusing electrostatic field. This directly influences the stability of the spatial distribution of the incident electron in the time domain [25]. However, to the best of our knowledge, there are few theoretical studies on backscattered electron characteristic in the EBCMOS.

In this paper, the backscattered electron characteristic in an EBCMOS were simulated by using Monte-Carlo method based on the principle of interactions between the high energy electrons and a solid. We assigned four parameters to describe the backscattered electron characteristics, and studied how these characteristics were affected by the surface structure of the BSB-CMOS and the incident electron energy. The effects of these backscattered electron characteristics on the EBCMOS performance (N_{BE} and resolution) were also discussed. This work will provide a theoretical foundation for the fabrication of high performance of EBCMOS.

Manuscript received 15 June 2022; revised 27 August 2022; accepted 19 October 2022. Date of publication 25 October 2022; date of current version 8 November 2022. This work was supported in part by the National Natural Science Foundation of China under Grant U2141239 and in part by the Science and Technology Research Project of Jilin Education Department under Grant JJKH20210800KJ. *(Corresponding authors: De Song; Weijun Chen.)*

Xuening Wang, De Song, Ye Li, and Weijun Chen are with the Changchun University of Science and Technology, Changchun, Jilin 130022, China (e-mail: wxn15633586106@163.com; songde614@163.com; liyecust@163.com; chenweijun@cust.edu.cn).

Gangcheng Jiao is with the Science and Technology on Low-Light-Level Night Vision Laboratory, Xi'an, Shanxi 710065, China (e-mail: jiaogc613@163.com).

Digital Object Identifier 10.1109/JPHOT.2022.3216873

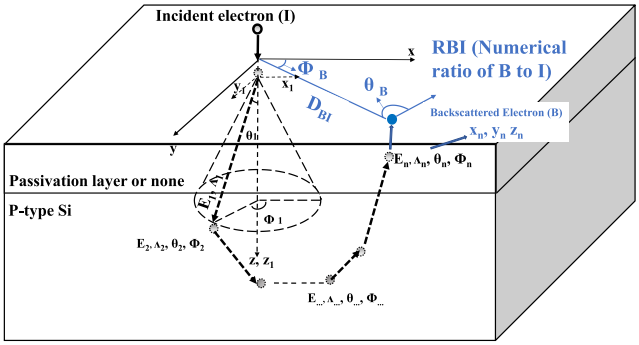

Fig. 1. Schematic diagram of an incident electron trajectory in the BSB-CMOS, and the corresponding parameters describing the backscattered electron characteristics: backscattered azimuth (Φ_{B}), backscattered angle (θ_{B}), the ratio of backscattered electron number to incident electron number (RBI), and the distance between the backscattered electron and incident electron (D_{BI}).

II. Physical Mode

Fig. 1 shows a schematic diagram of an incident electron trajectory in the BSB-CMOS and the parameters of the backscattered electron characteristics, which are the backscattered azimuth (Φ_{B}), backscattered angle (θ_{B}), the ratio of backscattered electron number to incident electron number (RBI), and the distance between the backscattered electron and incident electron (D_{BI}). To simulate the incident electron trajectory, the scattering angle (θ_{n}), scattering azimuth (Φ_{B}), scattering step (Λ_{n}), and residual energy (E_{n}) of an incident electron after the nth scattering can be calculated by (1)–(4) [26]. The energy of the incident electron is continuously reduced in the process of continuous collision, energy loss is calculated from Bethe energy-loss equation revised by Lou and Jay [26]. The cut-off energy of the moving electron traced in the MC simulation is 50eV.

$$\cos\theta_n = 1 - \frac{2\times 3.4\times 10^3 Z_{\mathrm{i}}^{2/3}\Big/E_{n-1}R}{1-3.4\times 10^3 Z_i^{2/3}\Big/E_{n-1}-R} \tag{1}$$

$$\Phi_{\mathrm{n}} = 2\pi R \tag{2}$$

$$\boldsymbol{\Lambda}_n = \frac{A}{N_A\rho\sigma_T}\ln R \tag{3}$$

$$E_n = E_{n-1} - 785\frac{\rho Z_i}{AE_{n-1}} \ln\left(\frac{1.166(E_{n-1}+t(9.76Z+58.5Z_i^{-0.19})\times 10^{-3})}{(9.76Z_i+58.5Z_i^{-0.19})\times 10^{-3}}\right)\Big|_{E_{n-1}}\cdot\boldsymbol{\Lambda}_{n-1} \tag{4}$$

Here R is a random number in the range (0, 1), Z_{i} is the ith atomic number, A is the atomic weight, N_{A} is the Avogadro constant, ρ is the density, E_0 is the initial energy of the incident electron, unit is eV and σ_{T} is the elastic scattering cross section calculated by

$$\sigma_{\mathrm{T}} = \frac{3.0\times 10^{-18} Z_i^{1.7}}{E_n + 0.005Z_i^{1.7}E_n^{0.5} + 0.007Z_i^2/E_n^{0.5}}. \tag{5}$$

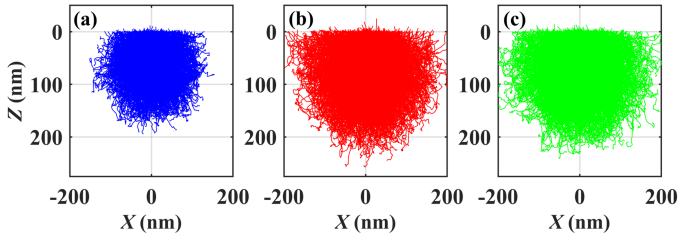

Fig. 2. The incident electron trajectories in the BSB-CMOS: (a) with Al_2O_3 passivation layer; (b) with SiO_2 passivation layer; (c) with barred passivation layer.

If the incident depth of an incident electron after its nth elastic collision with solid atoms changes from positive to negative, this would indicate that the incident electron has scattered back into the vacuum from the BSB-CMOS surface. The initial energy of the backscattered electrons can be calculated, which are equal to the energy when the incident electron is scattered into the vacuum. The value of them will also influence the re-incident distribution of backscattered electrons. The coordinates of the backscattered electron at its nth elastic collision can be calculated by (6), where $Q_{\mathrm{n}+10}$ (calculated by (7)) represents multiplication of the transition matrix from spherical coordinates to Cartesian coordinates at each collision.

$$\begin{bmatrix} x_0 \\ y_0 \\ z_0 \end{bmatrix} = Q_{n+1,0}\begin{bmatrix} x_{n+1} \\ y_{n+1} \\ z_{n+1} \end{bmatrix} \tag{6}$$

$$Q_{n+1,0} = Q_{0,0}\cdots Q_{n,n-1}\cdot Q_{n+1,n} = Q_{n,0}\cdot Q_{n+1,n} \tag{7}$$

$$Q_{n+1,n} = \begin{bmatrix} -\sin\varphi & -\cos\varphi\cos\theta & \cos\varphi\sin\theta \\ \cos\varphi & -\sin\varphi\cos\theta & \sin\varphi\cos\theta \\ 0 & \sin\theta & \cos\theta \end{bmatrix} \tag{8}$$

Next, the values of D_{BI}, θ_{B}, and Φ_{B} can be calculated by (9), where the subscripts n and $n+1$ are the elastic collision numbers. θ_{B} refers to the angle between the electron emission direction and the solid surface, and then the probability density is calculated to fit the distribution. Also, the distributions of D_{BI} and Φ_{B} can be obtained according to equations for the probability density.

$$\begin{aligned} D_{\mathrm{BI}} &= \sqrt{X_{n+1}^2 + Y_{n+1}^2} \\ \theta_{\mathrm{B}} &= \tan^{-1}\left(\frac{(Z_{n+1}-Z_n)}{\sqrt{(X_{n+1}-X_n)^2+(Y_{n+1}-Y_n)^2}}\right) \\ \Phi_{\mathrm{B}} &= \tan^{-1}\left(Y_{n+1}/X_{n+1}\right) \end{aligned} \tag{9}$$

III. Results and Discussion

A. The Influence of Passivation Layer Material on Backscattered Electron Characteristics

Fig. 2 shows the incident electron trajectories in the BSB-CMOS modified with 60 nm Al_2O_3, SiO_2, and a barred passivation layer, when the energy and diameter of the incident electron beam (Gaussian distribution) in the EBCMOS are assumed to be 4 keV and 20 nm (according to the reported range), respectively

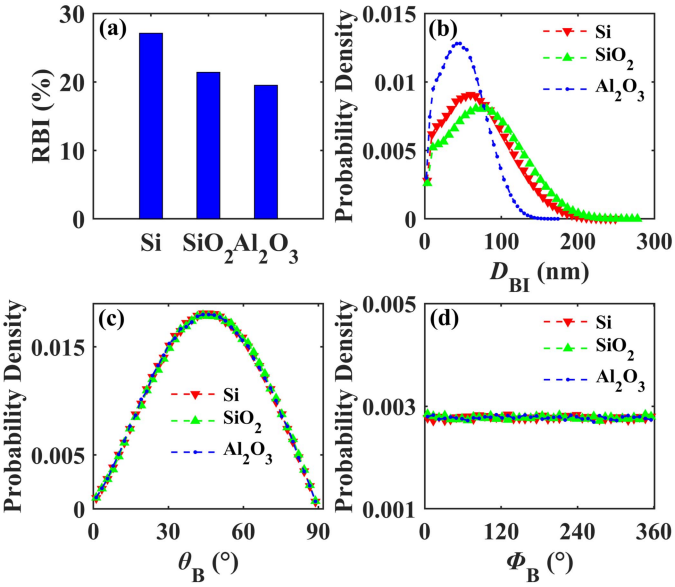

Fig. 3. The backscattered electron characteristics of device surfaces modified with barred, Al_2O_3, and SiO_2 passivation layers. (a) The distribution of the ratios of backscattered electron number to incident electron number (RBI). (b) The distribution of the distances between backscattered electrons and incident electrons (D_{BI}). (c) The distribution of θ_{B}. (d) The distribution of Φ_{B}.

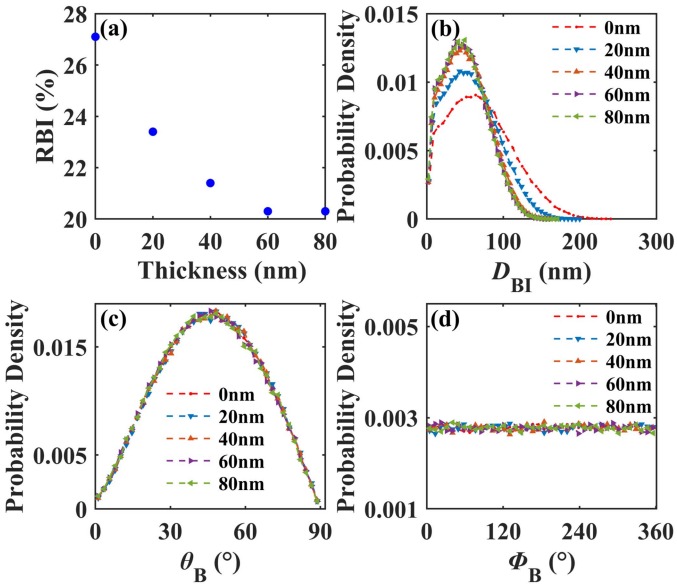

Fig. 4. The backscattered electron characteristics for the devices with different Al_2O_3 layer thickness. (a) The RBI vs thickness Al_2O_3 layer. (b) The distributions of D_{BI}. (c) The distributions of θ_{B}. (d) The distributions of Φ_{B}.

[5], [22]. Other parameters of the EBCMOS are assumed to the same, except the densities of Al_2O_3, SiO_2, and Si (3.8, 2.2, and 2.33 g/cm^3, respectively). The incident depth of the electrons and the scattering radius are smallest for the device with the Al_2O_3 passivation layer. This is mainly because of its highest density, which causes the mean electron scattering step size and energy loss of each elastic collision in Al_2O_3 passivation layer to be the largest. For the above three types of EBCMOS, the simulation results of the RBIs and the distributions of backscattered electrons with different thicknesses of the passivation layer are shown in Fig. 3. The RBIs are different for the three EBCMOS, and a lower RBI may reduce the device noise originating from the backscattered electrons (N_{BE}) due to the smaller number of backscattered electrons. The RBI was the lowest for the device with a modified with Al_2O_3 passivation layer. This is mainly because the probability of elastic scattering decreases by the order Si $>$ SiO_2 $>$ Al_2O_3, reflecting that the size of the elastic scattering cross section decreases as Si $>$ Al $>$ O according to (2). The average D_{BI} was the lowest for the device modified with the Al_2O_3 passivation layer, followed by the device with the barred passivation layer. This trend arises because the scattering step of the backscattered electrons in Al_2O_3 is shorter than that in the others, according to (3), due to the higher density of the Al_2O_3 passivation layer. Meanwhile, the lower mean D_{BI} may enhance the device resolution, because the distribution of the backscattered electrons beam is more concentrated. The distributions of θ_{B} for the three types of EBCMOS are very similar, and follow cosine angular distributions with a peak of 45 degrees, similar results have been reports in [27] and [28]. The distributions of Φ_{B} for the three types of EBCMOS are uniform, as can be deduced from (2). Therefore, the density and atomic number might be the key factors that affect the backscattered electrons characteristics. Specifically, N_{BE} and the resolution of the EBCMOS might be improved by a modified BSB-CMOS with high density passivation materials composed of substances with lower atomic number.

B. The Influence of Passivation Layer Thickness on Backscattered Electron Characteristics

Fig. 4 shows that the backscattered electron characteristics vary as the thickness of Al_2O_3 passivation layer increases, other parameters are the same as figure (3). As shown in Fig. 4(a), one can find that the RBI decreases with increasing Al_2O_3 layer thickness, because the RBI for the Si layer is larger than that for Al_2O_3, and the depths of the incident electrons are concentrated in the surface [10], [22]. Fig. 4(b) shows the distributions of D_{BI} for the devices with different Al_2O_3 layer thickness. The average D_{BI} decreases rapidly as the Al_2O_3 layer increases from 0 nm to 40 nm, and remains a steady distribution after 40 nm, because the incident depth of most incident electrons is 80 nm. The distributions of θ_{B} and Φ_{B} have no change with increasing the Al_2O_3 passivation layer thickness, as can be seen in Fig. 4(c) and (d).

C. The Influence of Incident Electron Energy on Backscattered Electron Characteristics

Fig. 5(a) shows the backscattered electron characteristics for the devices with a 60 nm Al_2O_3 layer, and varying incident electron energy. The diameter of the incident electron beam (Gaussian distribution) in the EBCMOS is assumed to be 20 nm, and the other parameters of the EBCMOS are assumed to be the same. The RBI shown in Fig. 5(a) first decreases and then increases. Meanwhile, the smallest RBI (20.3%) was obtained

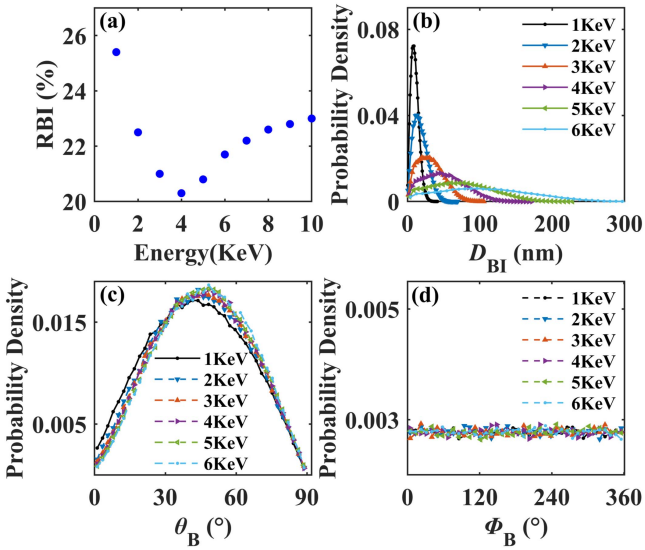

Fig. 5. The backscattered electron characteristics for devices with varying incident energy. (a) RBI vs incident energy. (b) The distributions of D_{BI}. (c) The distributions of θ_{B}. (d) The distributions of Φ_{B}.

for the incident electron energy of 4 keV. In the decreasing stage, when the incident energy is smaller than 4 keV, the incident electrons in the passivation layer will be more easily elastically scattered because the elastic scattering cross-section decreases with increasing incident energy according to (5). When the incident energy is between 4 keV and 10 keV, the incident electrons are elastically scattered in the Si substrates and Al_2O_3 layer, respectively. As the energy increases, most of electrons are elastically scattered in the Si substrate, and the elastic scattering cross-section of Si is larger than Al_2O_3, which leads to the increase of the RBI. Fig. 5(b)–(d) shows the D_{BI}, Φ_{B} and θ_{B} distributions of backscattered electrons for incident electrons with different values of energy. The mean D_{BI} increases clearly as the incident energy increases. The distributions of Φ_{B} with varying incident energy are uniform. The distributions of θ_{B} follow cosine angular distributions with a peak of 45 degrees.

Therefore, a lower incident energy is optimal for EBCMOS applications. However, the lower energy will enhance the backscattered ratio, which impairs the gain of the electron multiplication layer.

IV. Conclusion

The backscattering model in the EBCMOS was established based on the principle of electron-solid interactions as well as Monte Carlo simulation. We studied how the backscattered electron characteristics are affected by the surface structure of BSB-CMOS and incident electron energy. Firstly, compared to devices with no passivation layer, our results show that the RBI and the mean D_{BI} are reduced by adding the passivation layer. Secondly, with increasing passivation layer thickness, the RBI and the mean D_{BI} will decrease rapidly at first, then slowly, and eventually becoming steady distribution. Finally, as incident electron energy increases, RBI decreases rapidly at first, and then slowly increases. However, the mean D_{BI} will increase rapidly with increasing incident electron energy. Furthermore, the distributions of Φ_{B} and θ_{B} remain constant when adding different passivation layers. Overall, the lowest RBI and a low mean value of D_{BI} were achieved when the BSB-CMOS surface was modified with 60 nm Al_2O_3 and the incident electron was 4 keV, which might improve the N_{BE} and resolution of the EBCMOS. Therefore, this study will provide a theoretical foundation for the fabrication of high-resolution image devices based on the study of backscattered electron characteristic in EBCMOS.

References

[1] V. W. Aebi and J. J. Boyle, "Electron bombarded active pixelsensor," U.S. Patent 6285018B1, Sep. 04, 2001.

[2] L. M. Hirvonen and K. Suhling, "Photon counting imaging with an electron-bombarded pixel image sensor," *Sensors*, vol. 16, no. 5, Apr. 2016, Art. no. 617.

[3] V. W. Aebi, K. A. Costello, P. W. Arcuni, P. Genis, and S. J. Gustafson, "EBAPS: Next generation, low power, digital night vision," in *Proc. OPTRO Int. Symp.*, 2005, pp. 1–10.

[4] J. A. Levitt et al., "Fluorescence anisotropy of molecular rotors," *Chem. Phys. Chem.*, vol. 12, no. 3, pp. 662–672, 2011.

[5] H. L. Liu et al., "High resolution electron bombareded complementary metal oxide semiconductor sensor for ultraviolet detection," *Acta Physica Sinica*, vol. 67, no. 1, pp. 1–6, 2018, Art. no. 014209.

[6] S. B. Sobottka et al., "Evaluation of the clinical practicability of intraoperative optical imaging comparing three different camera setups," *Biomedizinische Technik*, vol. 58, no. 3, pp. 237–248, 2013.

[7] A. Dominjon et al., "An ebCMOS camera system for marine bioluminescence observation: The luSEapher prototype," *Nucl. Instrum. Methods Phys. Res. Sect. A*, vol. 695, pp. 172–178, Nov. 2012.

[8] R. Barbier et al., "First results from the development of a new generation of hybrid photon detector: EBCMOS," in *Proc. 10th Conf. Astroparticle, Part., Space Phys., Detectors Med. Phys. Appl.*, 2007, pp. 23–27.

[9] J. F. Tian, D. Song, W. J. Chen, and Y. Li, "Influence of doping distribution in electron multiplier surface layer on charge collection efficiency of EBCMOS," *Semicond. Optoelectron.*, vol. 42, pp. 45–51, 2021.

[10] S. De, S. Feng, and L. Ye, "Simulation of charge collection efficiency for EBAPS with uniformly doped substrate," *Infrared Laser Eng.*, vol. 45, no. 2, Feb. 2016, Art. no. 0203002.

[11] D. Song, J. Q. Zhou, Y. Mu, H. Cheng, and H. Fan, "Testing system of multiplying electron gain for electron bombarded semiconductor," *Proc. SPIE*, vol. 10697, 2018, Art. no. 106970T.

[12] A. Dominjon et al., "LUSIPHER large-scale ultra-fast single photoelectron tracker," in *Proc. IEEE Nucl. Sci. Symp. Conf. Rec.*, 2009, pp. 1527–1531.

[13] R. Barbier et al., "A single-photon sensitive ebCMOS camera: The LUSIPHER prototype," *Nucl. Instrum. Methods Phys. Res. Sect. A*, vol. 648, no. 1, pp. 266–274, Apr. 2011.

[14] A. Hussain et al., "Monte Carlo simulation study of electron yields from compound semiconductor materials," *J. Appl. Phys.*, vol. 128, Jul. 2020, Art. no. 015305.

[15] M. Hannachi, Z. Rouabah, C. Champion, and N. Bouarissa, "Electron backscattering from solid targets: Elastic scattering calculations," *J. Electron Spectrosc. Related Phenomena*, vol. 195, pp. 155–159, Jul. 2014.

[16] R. Shimizu and D. Ze-Jun, "Monte Carlo modelling of electron-solid interactions," *Rep. Prog. Phys.*, vol. 55, no. 4, pp. 487–531, 1992.

[17] A. Bentabet and N. Fenineche, "Backscattering coefficients for low energy positrons and electrons impinging on bulk solid targets," *J. Phys.: Condens. Matter*, vol. 21, no. 9, Jan. 2009, Art. no. 095403.

[18] M. Dapor, N. Bazzanella, L. Toniutti, A. Miotello, and S. Gialanella, "Backscattered electrons from surface films deposited on bulk targets: A comparison between computational and experimental results," *Nucl. Instrum. Methods Phys. Res., Sect. B*, vol. 269, no. 14, pp. 1672–1674, Jul. 2011.

[19] L. Yang, A. Hussain, S. Mao, B. Da, K. Tőkési, and Z. J. Ding, "Electron backscattering coefficients of molybdenum and tungsten based on the Monte Carlo simulations," *J. Nucl. Mater.*, vol. 553, May. 2021, Art. no. 153042.

[20] S. C. Fu, B. Sun, Q. Wang, G. C. Jiao, L. Feng, and Y. Li, "Simulations on the electron back-scattering characteristics of ion barrier film," *Proc. SPIE*, vol. 8912, 2013, Art. no. 89120P.

[21] S. C. Fu, Y. Li, F. Shi, Z. Miao, H. Cheng, and Q. Duanmu, "Simulation and detection of electron back-scattering in ion barrier films of micro-channel plate," *Proc. SPIE*, vol. 9521, 2015, Art. no. 952109.

[22] J. Z. Bai et al., "The analysis of electron scattering among multiplying layer in EBAPS using optimized Monte Carlo method," *Modern Phys. Lett. B*, vol. 34, Sep. 2020, Art. no. 2050398.

[23] J. Z. Bai et al., "Optimum design of electron bombarded active pixel sensor for low-level light single photon imaging," *Proc. SPIE*, vol. 10843, Feb. 2019, Art. no. 108430V.

[24] X. Piao et al., "Simulation of multiplying electron distribution in electron multiplier layer for EBAPS," *Proc. SPIE*, vol. 10141, 2016, Art. no. 101410W.

[25] W. Wang, Y. Li, W. Chen, D. Song, and X. Wang, "Simulation of the electrostatic distribution in the proximity focusing structure of an EBCMOS," *IEEE Photon. J,* vol. 12, no. 3, Jun. 2020, Art. no. 6901210.

[26] R. Browning et al., "Empirical forms for the electron/atom elastic scattering cross sections from 0.1 to 30 keV," *J. Appl. Phys.*, vol. 76, no. 4, pp. 2016–2022, Apr. 1994.

[27] J. I. Goldstein, D. E. Newbury, J. R. Michael, N. W. M. Ritchie, J. H. J. Scott, and D. C. Joy, "Backscattered electrons," in *Scanning Electron Microscopy and X-Ray Microanalysis*. New York, NY, USA: Springer, 2018, pp. 15–28.

[28] A. Hussain, L. Yang, S. Mao, B. Da, K. Tőkési, and Z. J. Ding, "Determination of electron backscattering coefficient of beryllium by a high-precision Monte Carlo simulation," *Nucl. Mater. Energy*, vol. 26, 2021, Art. no. 100862.